TIME DOMAIN OUTPUT ERROR SYSTEM IDENTIFICATION OF ICED AIRCRAFT AERODYNAMICS

C. Deiler, German Aerospace Center (DLR), Institute of Flight Systems
Lilienthalplatz 7, 38108 Braunschweig, Germany

Abstract

A Δ-model approach to characterize changed aircraft dynamics due to icing is analytically derived and its parameters are estimated. The model extension is formulated as a separate module in the aircraft flight mechanics simulation and can be used in existing simulation models. The application of the output error method in time domain allows to satisfactorily match model outputs and measurements as well as calculated aerodynamic derivatives. Using available flight data of a light business jet with different ice accumulation cases provided by EMBRAER, model parameters of the Δ-model are determined and interpreted pertaining to the aerodynamic degradation caused by icing. The results show good promise, that the combination of modeling approach and estimation technique could be applicable to extend existing simulator models providing a basis for pilot training under icing conditions.

NOMENCLATURE

Symbols

a	model parameter	
α	angle of attack	rad
$\dot{\alpha}^*$	non-dimensional rate change of angle of attack	
a_x,a_z	accelerations in x, z direction	m/s^2
$\bar{c}$	mean aerodynamic chord	m
C	aerodynamic coefficient	
c_1, $\alpha^\star$	flow separation function parameters	
D	drag force	N
d	icing model offset	
e	Oswald factor	
ε	downwash angle	rad
η	elevator deflection	rad
f,g	nonlinear system functions	
g	acceleration due to gravity	m/s^2
H	altitude	m
i	index	
i_{HT}	horizontal tail plane deflection	rad
I_{xx}, I_{yy}, I_{zz}, I_{xz}	moments of inertia	Nm^2
J	cost function	
k	icing model factor	
k_1, k_2, k_4	drag coefficient factors	
L	lift force	N
Λ	wing aspect ratio	-
L, M, N	body fixed moments about x,y,z axis	Nm
m	mass	kg
Ma	Mach number	1
N	number of data points	
ν	measurement noise	
P	model parameter	
Φ, Θ, Ψ	Euler angles	rad
p,q,r	rotational velocities	rad/s
R	covariance matrix of measurement noise	
r_{HT}, $r^\star_{HT}$, $z^\star_{HT}$	horizontal tail lever arms	m
S	surface area	m^2

σ	standard deviation	
t	time	s
τ_2	time constant	1/s
Δt	time delay	s
T_f	inertia tensor	
Θ_p	parameter vector	
u	input vector	
u,v,w	translational velocities along x,y,z axis	m/s
V_{TAS}	true airspeed	m/s
x	state vector	
ξ	aileron deflection	rad
$\widehat{X}$	wing flow separation point	
X, Y, Z	body fixed forces along x,y,z axis	N
y	simulated output vector	
z	measured output vector	

Subscripts

A	aerodynamic
Base	base model part
E	engine
HT	horizontal tail
Ice	Δ-model part (icing)
WB	wing/body

1 INTRODUCTION

Icing can have hazardous effects on the aircraft performance characteristics. Moreover aircraft operational limitations must be adapted to maintain a safe flight envelope. Nevertheless, dynamic behavior change and possible premature stall increase the need for pilot situational awareness and an adaption of any aircraft control strategy.

During the last decades various accidents worldwide have shown the severity of icing related degradations as well as pilot's difficulties to cope with changes in aircraft behavior ([1, 2, 3]). The main degradation due to aerodynamic icing manifests itself in a reduced stall angle of attack and increased drag (see Fig. 1). Various studies on these effects for different airfoils and icing cases

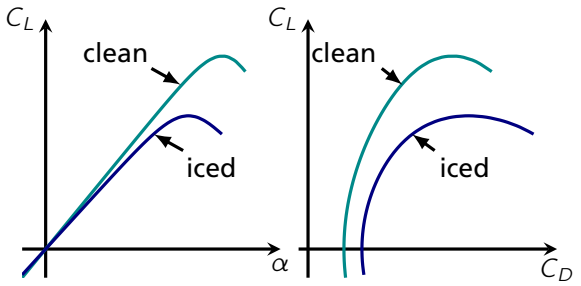

Figure 1: Expected aerodynamic degradation due to icing [5] (lift curve and drag polar)

(e.g. [4, 5, 6]) as well as for complete aircraft (e.g. [7, 8, 9, 10]) had been conducted in the past.

From a scientific point of view different aspects of the aircraft icing phenomena are of interest. For example:

1. aircraft limitations and behavior with accumulated ice on different surfaces
2. flight performance, dynamic behavior and handling quality changes during ice accretion
3. aircraft behavior with variable accumulation severity over different surfaces
4. aircraft behavior during de-icing and ice shedding
5. pilot's situational awareness concerning icing and ability to detect a contamination

The challenge in describing aerodynamic degradations mathematically is to combine points 1-4 in one model formulation to extend the aerodynamics in the simulation. For dynamic simulation analysis or training in a flight simulator the model must be capable of accumulating ice on certain aircraft parts and/or de-icing the aircraft if e.g the aircraft leaves atmospheric icing conditions or countermeasures are activated.

This paper mainly addresses to item 1 of describing the aircraft limitations and behavior using flight data for model development using system identification techniques. In several attempts, the aircraft icing degradation problem had been faced based on data collected at the beginning of the last decade [11, 12, 13, 14]. With notable success, the aerodynamic model formulations had been changed and extended for reliably considering icing effects and this built-in approach was used to develop a special icing training simulator[13, 15]. Parameters of these models were mainly estimated with equation-error regression techniques (e.g. in [16]) resulting in a good match of aerodynamic coefficients but not necessarily matching dynamic system outputs, which are mandatory for a trustworthy and validated dynamic model behavior in e.g. training simulators.

Another way for accounting the degradation in the simulation model is to extend an available basic aircraft model with an additional part (Δ-model) in the aerodynamics module [17]. After a basic aircraft simulation model is formulated, identified and validated for a specific aircraft, extensions for covering aerodynamic icing effects are derived to estimate and afterwards simulate performance changes. This approach gives the advantage that existing aerodynamic models do not have to be altered and the module parameters can be independently determined from the data source. It is possible to use flight data for the parameter estimation process, as well as information about additional icing related forces resulting from CFD calculations because the Δ-model induced changes are superimposed upon the basic aerodynamic forces resp. their derivatives. An illustration about the extension of the basic model formulations is given in Fig. 2.

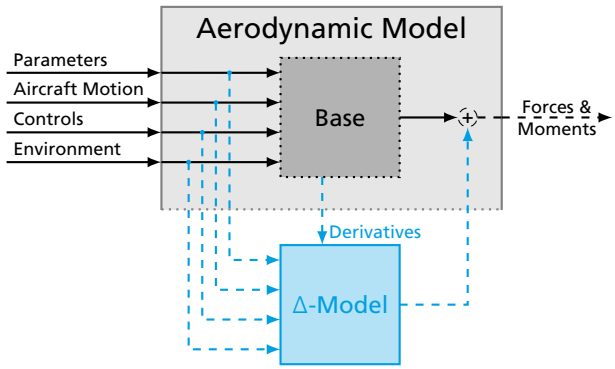

Figure 2: Illustration of aerodynamic model with Δ-model extension

Using the output error method in time domain to estimate the corresponding model parameter values guarantees the best possible match of simulated and measured outputs. This match of the altered dynamic behavior is mandatory to e.g. develop new strategies for enhancing a pilot's situational awareness concerning aircraft icing.

The herein presented Δ-model extension covers ice related changes of the longitudinal motion aerodynamics in lift, drag and pitching moment. Changes contributing the basic stall model formulation and the drag polar curvature are necessary to cover icing effects. Using a base model formulation splitting aircraft wing and horizontal tail influences for the pitching moment calculation (2-point model[18]), the Δ-model is designed to also consider changed horizontal tail aerodynamics due to inflow changes and/or accumulated ice. The fundamental Δ-model formulation for icing effects is comparable to the model proposed in [11], where model parameters are linearly altered to include icing related aerodynamic degradations.

To demonstrate the capability of the proposed Δ-model to reproduce aerodynamic icing effects in the aircraft simulation, existing flight data under two different icing conditions (different artificial ice shapes on wing and tail surfaces) of a light business jet are used to estimate Δ-model parameters. The flight data are provided by EMBRAER as a part of a scientific exchange on aircraft icing with DLR Institute of Flight Systems.

During the system identification process the DLR software Fitlab is used for parameter estimation. The software includes a maximum likelihood parameter estimation method formulation in time domain with a Gauss-Newton optimization algorithm implementation.

2 OUTPUT ERROR PARAMETER ESTIMATION IN TIME DOMAIN

The Output Error Method in time domain (iterative maximum likelihood method) is selected for parameter estimation because of its capability of computing the most likely parameters of a complex nonlinear aircraft simulation model. The formulation of a general nonlinear aircraft model is given by

$$\begin{aligned} \dot{x}(t) &= f(x(t), u(t), \Theta_p), \quad x_0 = x(t_0) \\ y(t) &= g(x(t), u(t), \Theta_p). \end{aligned} \tag{1}$$

where x denotes the aircraft states and y the observations, u is the control input vector, and f, g are nonlinear functions describing the system's behavior. The output measurements z are sampled at N time steps and contain Gaussian white noise with zero mean ν and the covariance matrix R:

$$z(t_i) = y(t_i) + \nu(t_i), \quad i \in [1, N]. \tag{2}$$

With the measurement noise covariance matrix given by the residuals of measurement and simulated observation at each point

$$R = \frac{1}{N} \sum_{i=1}^{N} [z(t_i) - y(t_i)] [z(t_i) - y(t_i)]^T, \tag{3}$$

the estimation cost function – as the negative logarithm of the probability density of measurements z for a given parameter vector Θ_p – can be expressed as follows

$$J(\Theta_p) = \det(R). \tag{4}$$

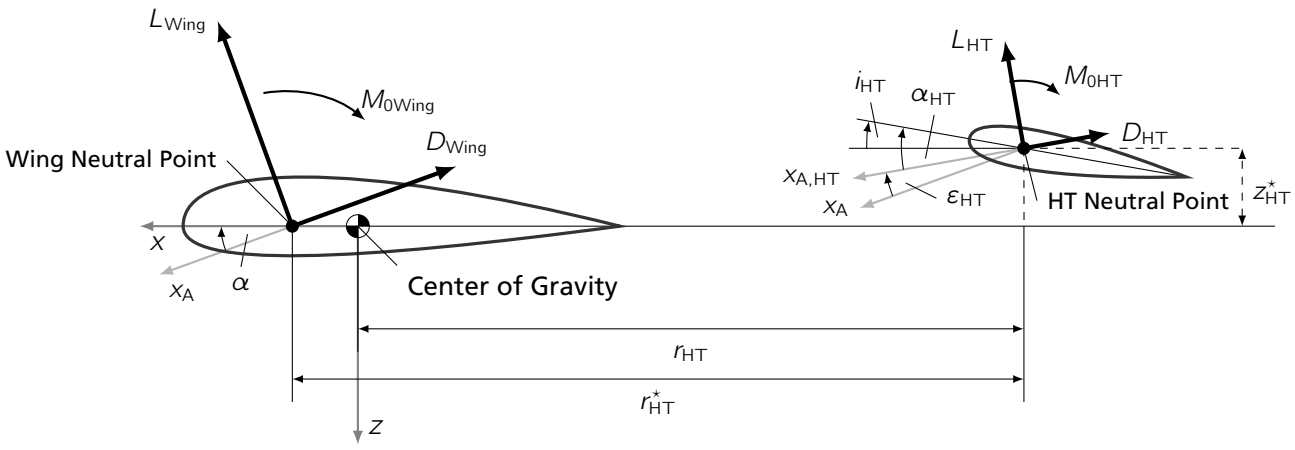

Figure 3: Illustration wing and horizontal tail geometry for the two-point model formulation [18]

This function can be minimized using state of the art optimization approaches like a Gauss-Newton algorithm. For any further information on this specific parameter estimation approach the reader is referred to the work of Jategaonkar [17, 19].

The resulting iterative output error parameter estimation algorithm is part of the DLR parameter estimation software "Fitlab".

3 BASIC MODEL FORMULATION

The basic aircraft motion is represented by a 6 DOF kinematic model. The equations of the translational motion are given by

$$\begin{aligned} \dot{u} &= -q \cdot w + r \cdot v - g \sin\Theta \qquad + \frac{X_E + X_A}{m} \\ \dot{v} &= -r \cdot u + p \cdot w + g \cos\Theta \sin\Phi + \frac{Y_E + Y_A}{m} \\ \dot{w} &= -p \cdot v + q \cdot u + g \cos\Theta \cos\Phi + \frac{Z_E + Z_A}{m}, \end{aligned} \tag{5}$$

where the engine forces are denoted by X_E, Y_E, Z_E. The unsteady nonlinear aerodynamic model influence is represented by the forces X_A, Y_A, Z_A in the corresponding direction. With the inverse inertia tensor

$$T_f^{-1} = \begin{bmatrix} I_{xx} & 0 & -I_{xz} \\ 0 & I_{yy} & 0 \\ -I_{xz} & 0 & I_{zz} \end{bmatrix}_f^{-1} \tag{6}$$

the rotational motion equations are given by

$$\begin{aligned} \begin{bmatrix} \dot{p} \\ \dot{q} \\ \dot{r} \end{bmatrix}_f = & T_f^{-1} \left(\begin{bmatrix} L_E + L_A \\ M_E + M_A \\ N_E + N_A \end{bmatrix}_f \right. \\ & \left. - \begin{bmatrix} qr(I_{zz} - I_{yy}) - pqI_{xz} \\ rp(I_{xx} - I_{zz}) + (p^2 - r^2)I_{xz} \\ pq(I_{yy} - I_{xx}) + qrI_{xz} \end{bmatrix}_f \right) \end{aligned} \tag{7}$$

including engine induced body fixed moments L_E, M_E, N_E and aerodynamic moments L_A, M_A, N_A.

A two-point aerodynamic model implementation [18] separating wing and horizontal tail influences is used to represent the unsteady nonlinear aerodynamics of the longitudinal motion. Figure 3 gives an illustration of the geometry and the aerodynamic forces and moments at wing and horizontal tail. The separation allows to easily consider nonlinearities like downwash or flow transit time effects between wing and tail. The complete model equations are outlined in [18] and used for the Δ-model derivation hereafter. To represent an unsteady nonlinear stall behavior by the two-point model, the equation are extended according to the formulations in [20, 21, 22].

The non-dimensional wing flow separation $\widehat{X}$ is given by [20]

$$\widehat{X} = \frac{1}{2} \cdot \left(1 - \tanh\left(c_1 \cdot (\alpha - \tau_2 \dot{\alpha}^* - \alpha^\star)\right)\right) \tag{8}$$

with the non-dimensional angle of attack time derivative

$$\dot{\alpha}^* = \dot{\alpha} \frac{\bar{c}}{V_{TAS}}. \tag{9}$$

The simplified wing/body lift coefficient equation including stall results in

$$C_{L,WB} = C_{L0} + C_{L\alpha,WB} \cdot \left(\frac{1 + \sqrt{\widehat{X}}}{2} \right)^2 \alpha \tag{10}$$

considering herein only zero lift and angle of attack dependent lift parts. The basic horizontal tail lift coefficient equation is given by

$$C_{L,HT} = C_{L\alpha,HT} \cdot \alpha_{HT} + C_{L\eta} \cdot \eta. \tag{11}$$

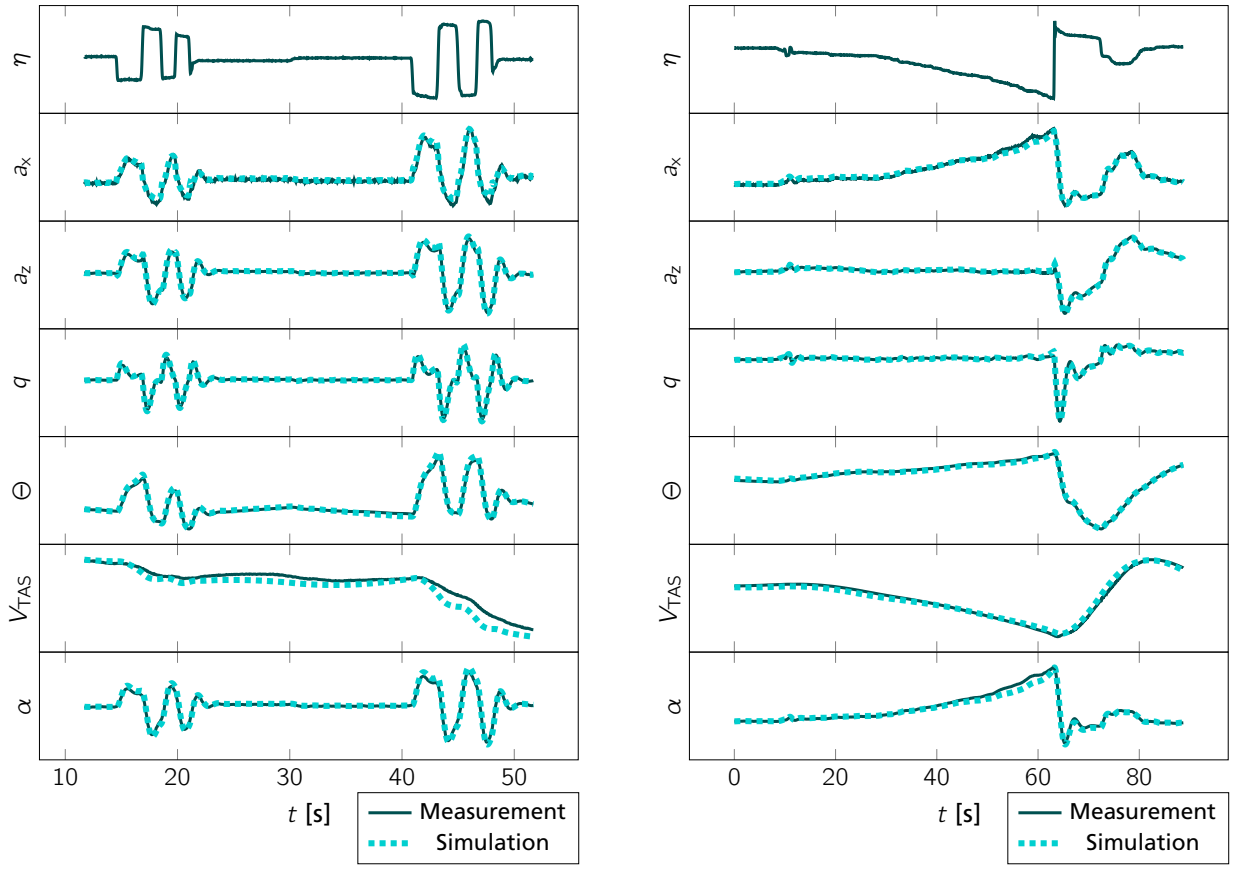

(a) Elevator 3-2-1-1 multistep input maneuver

(b) Stall Approach

Figure 4: Time history of basic aircraft reaction – measurement and simulation of outputs

The geometric relations in Fig. 3 yield the horizontal tailplane angle of attack

$$\alpha_{\mathrm{HT}} = \alpha + i_{\mathrm{HT}} - \varepsilon_{\mathrm{HT}} + \arctan\left(\frac{q \cdot r_{\mathrm{HT}}}{V_{\mathrm{TAS}}}\right), \qquad (12)$$

where the downwash angle is formulated as

$$\begin{aligned}\varepsilon_{\mathrm{HT}} = & \frac{\partial \varepsilon_{\mathrm{HT}}}{\partial \alpha} \cdot \alpha(t - \Delta t) \\ & + \frac{\partial \varepsilon_{\mathrm{HT}}}{\partial \widehat{X}} \cdot \left(1 - \widehat{X}(t - \Delta t)\right).\end{aligned} \qquad (13)$$

The complete lift coefficient results from wing/body ($C_{L,\mathrm{WB}}$) and horizontal tail part ($C_{L,\mathrm{HT}}$)

$$C_L = C_{L,\mathrm{WB}} + \frac{S_{\mathrm{HT}}}{S_{\mathrm{Wing}}} C_{L,\mathrm{HT}}. \qquad (14)$$

The basic drag equation is dominated by zero, lift induced and stall dependent drag and can be expressed by

$$C_D = C_{D0} + \frac{1}{e\pi\Lambda} C_{L+}^2 \frac{\partial C_D}{\partial \widehat{X}} \left(1 - \widehat{X}\right). \qquad (15)$$

With calculating the body fixed forces coefficients $C_{X\mathrm{HT}}$ and $C_{Z\mathrm{HT}}$ from horizontal tail lift $C_{L,\mathrm{HT}}$ the basic pitching moment equations results in

$$\begin{aligned}C_m = & C_{m0,\mathrm{WB}} + \frac{S_{\mathrm{HT}}}{S_{\mathrm{Wing}}} \left(C_{Z\mathrm{HT}} \frac{r^\star_{\mathrm{HT}}}{\bar{c}} - C_{X\mathrm{HT}} \frac{z^\star_{\mathrm{HT}}}{\bar{c}}\right) \\ & + C_{mq,\mathrm{WB}} \frac{q\bar{c}}{V_{\mathrm{TAS}}} + \frac{\partial C_m}{\partial \widehat{X}} \left(1 - \widehat{X}\right).\end{aligned} \qquad (16)$$

The lateral motion aerodynamics are formulated as nonlinear derivative model. Such a model has been identified from flight data (see section 5) without any icing. Typically, 30 flight maneuvers pertaining to longitudinal motion such as 3-2-1-1 elevator multi step inputs, elevator step inputs and stall approaches were analyzed to estimate the parameters appearing in Eqs. (8) - (16).

To visualize the basic model quality a comparison of several measured and simulated outputs are given in Figure 4 for two different sample maneuvers. Figure 4a shows the time history of a typical system identification maneuver with an elevator 3-2-1-1 multistep input . The basic model is able to well match the measurements in terms of steady and dynamic behavior. The aircraft reaction during a stall approach – complete stall is not entered – is given in Figure 4b. It shows that the basic model is

able to cover the aircraft motion over a large angle of attack range and also the dynamic aircraft behavior during maneuver abortion.

4 Δ-MODEL FORMULATION

The aerodynamic Δ-model accounting for additional icing effects is analytically derived from the basic aerodynamic model equations in section 3. In the first step major effects on the longitudinal motion are considered and the equations are formulated to alter the corresponding aerodynamics of the two-point model.

The basic idea of using linear altered parameters for iced aerodynamics in aircraft simulation was initially introduced by Bragg [11]. For an arbitrary parameter in the derivative model the complete value P including a basic model part P_{Base} and an additional Δ-model part ΔP_{Ice} can be expressed as

$$P = P_{\text{Base}} + \Delta P_{\text{Ice}} = (1 + k_P) \cdot P_{\text{Base}} + d_P \tag{17}$$

using an additional factor k_P and a herein introduced offset d_P to model the degraded aircraft aerodynamics. To separate the aerodynamic degradation due to icing from the basic model equations, the Δ coefficient approach in Eq. (17) is used on all major model parameters in Eqs. (8) - (16). Within the process of model development it was found not useful to extend each model parameter with the formulation given in Eq. (17). Factors or offsets which are intended to have zero values are neglected in the following derivation.

Based on Eq. (17), the flow separation model parameters in Eq. (8) are expressed as

$$\begin{aligned} \tau_2 &= (1 + k_{\tau_2}) \cdot \tau_{2\text{Base}} \\ c_1 &= (1 + k_{c_1}) \cdot c_{1\text{Base}} \\ \alpha^\star &= (1 + k_{\alpha^\star}) \cdot {\alpha^\star}_{\text{Base}}. \end{aligned} \tag{18}$$

Substitution of these parameters in Eq. (8) leads to a separation of the hyperbolic tangent argument in its basic part $a_{1\text{Base}}$

$$a_{1\text{Base}} = c_{1\text{Base}} \cdot (\alpha - \tau_{2\text{Base}} \dot{\alpha}^* - {\alpha^\star}_{\text{Base}}) \tag{19}$$

and its icing part $a_{1\text{Ice}}$

$$\begin{aligned} a_{1\text{Ice}} = & c_{1\text{Base}} \cdot \left[k_{c_1} \alpha - {\alpha^\star}_{\text{Base}} \left(k_{c_1} + k_{\alpha^\star} \left(1 + k_{c_1} \right) \right) \right. \\ & \left. - \tau_{2\text{Base}} \dot{\alpha}^* \left(k_{c_1} + k_{\tau_2} \left(1 + k_{c_1} \right) \right) \right]. \end{aligned} \tag{20}$$

With

$$\widehat{X} = \widehat{X}_{\text{Base}} + \Delta \widehat{X}_{\text{Ice}} \tag{21}$$

and Eq. (8) the above equations yield the basic part $\widehat{X}_{\text{Base}}$ of the flow separation (similar Eq. (8)) and the icing induced influence

$$\Delta \widehat{X}_{\text{Ice}} = -0.5 \cdot \frac{\tanh(a_{1\text{Ice}}) - c_{1\,\text{Base}}^2 \tanh(a_{1\text{Ice}})}{1 + c_{1\text{Base}} \tanh(a_{1\text{Ice}})}. \tag{22}$$

Usage of Eq. (21) in Eq. (10) yields an additional ice induced wing/body lift coefficient part

$$\begin{aligned} \Delta C_{L,\text{WB}\,\text{Ice}} = \quad & k_{C_{L0}} C_{L0\,\text{Base}} \\ & + (a_{2\text{Base}} + a_{2\text{Ice}}) k_{C_{L\alpha,\text{WB}}} C_{L\alpha,\text{WB}\,\text{Base}} \alpha \\ & + a_{2\text{Ice}} C_{L\alpha,\text{WB}\,\text{Base}} \alpha \end{aligned} \tag{23}$$

with the parameter extensions

$$\begin{aligned} C_{L0} &= (1 + k_{C_{L0}}) \cdot C_{L0\,\text{Base}} \\ C_{L\alpha,\text{WB}} &= \left(1 + k_{C_{L\alpha,\text{WB}}}\right) \cdot C_{L\alpha,\text{WB}\,\text{Base}} \end{aligned} \tag{24}$$

and flow separation point influences

$$a_{2\text{Base}} = 0.25 \cdot \left(1 + 2\sqrt{\widehat{X}_{\text{Base}}} + \widehat{X}_{\text{Base}} \right) \tag{25}$$

$$\begin{aligned} a_{2\text{Ice}} = 0.25 \cdot \Bigg(& 2\sqrt{\widehat{X}_{\text{Base}} + \Delta \widehat{X}_{\text{Ice}}} \\ & - 2\sqrt{\widehat{X}_{\text{Base}}} + \Delta \widehat{X}_{\text{Ice}} \Bigg). \end{aligned} \tag{26}$$

The iced aerodynamic's lift curve slope is found to be not necessarily steady, so the lift coefficient factors $k_{C_{L0}}$ and $k_{C_{L\alpha,\text{WB}}}$ are used to introduce a lift curve breakpoint at α_{BP} as

$$\begin{aligned} k_{C_{L0}} &= \begin{cases} k_{C_{L0},\text{low}} & \text{if} \quad \alpha \leq \alpha_{\text{BP}} \\ k_{C_{L0},\text{high}} & \text{if} \quad \alpha > \alpha_{\text{BP}} \end{cases} \\ k_{C_{L\alpha,\text{WB}}} &= \begin{cases} k_{C_{L\alpha,\text{WB}},\text{low}} & \text{if} \quad \alpha \leq \alpha_{\text{BP}} \\ k_{C_{L\alpha,\text{WB}},\text{high}} & \text{if} \quad \alpha > \alpha_{\text{BP}} \end{cases} \end{aligned} \tag{27}$$

with

$$\begin{aligned} k_{C_{L0},\text{high}} = & k_{C_{L0},\text{low}} \\ & + \left(a_{2\text{Base}}(\alpha_{\text{BP}}) + a_{2\text{Ice}}(\alpha_{\text{BP}}) \right) \cdot \alpha_{\text{BP}} \\ & \cdot \left(k_{C_{L\alpha,\text{WB}},\text{low}} - k_{C_{L\alpha,\text{WB}},\text{high}} \right) \cdot \frac{C_{L\alpha,\text{WB}\,\text{Base}}}{C_{L0\,\text{Base}}}. \end{aligned} \tag{28}$$

Aerodynamic icing mainly influences the aircraft drag and hence the drag equation must be extended in several ways. On the one hand, parameters of the basic formulation in Eq. (15) must be considered for alteration. On the other hand also some model equation extensions to change the basic quadratic polar into a 4th order curve:

$$\begin{aligned} C_{D0} &= (1 + k_{C_{D0}}) \cdot (C_{D0})_{\text{Base}} \\ k_1 &= d_{k_1} \\ \frac{1}{e\Lambda\pi} &= \frac{(1 + k_{k_2})}{e_{\text{Base}}\Lambda\pi} + \frac{d_{k_2}}{e_{\text{Base}}\Lambda\pi} \\ k_4 &= d_{k_4} \\ \frac{\partial C_D}{\partial \widehat{X}} &= \left(1 + k_{\frac{\partial C_D}{\partial \widehat{X}}} \right) \cdot \left(\frac{\partial C_D}{\partial \widehat{X}} \right)_{\text{Base}}. \end{aligned} \tag{29}$$

The drag coefficient icing part $\Delta C_{D\text{Ice}}$ is given by

$$\begin{aligned}\Delta C_{D\text{Ice}} = \; & k_{C_{D0}} C_{D0\text{Base}} \\ & + \Delta C^2_{L,\text{WBIce}} \frac{k_{k_2}}{e\Lambda\pi} \\ & + C_{L\text{Base}} \cdot \Delta C_{L,\text{WBIce}} \frac{k_{k_2}}{e\Lambda\pi} \\ & + \left(C_{L\text{Base}} + \Delta C_{L,\text{WBIce}}\right) d_{k_1} \\ & + \left(C_{L\text{Base}} + \Delta C_{L,\text{WBIce}}\right)^2 \frac{d_{k_2}}{e\Lambda\pi} \\ & + \left(C_{L\text{Base}} + \Delta C_{L,\text{WBIce}}\right)^4 d_{k_4} \\ & + \left(k_{\frac{\partial C_D}{\partial \widehat{X}}} \left(1 - \left(\Delta \widehat{X}_{\text{Ice}} + \widehat{X}_{\text{Base}}\right)\right) \right. \\ & \qquad \left. - \Delta \widehat{X}_{\text{Ice}} \right) \left(\frac{\partial C_D}{\partial \widehat{X}}\right)_{\text{Base}}\end{aligned} \tag{30}$$

Note that due to the altered flow over the wing, a significant influence on the ailerons can be detected for some icing cases [23]. Therefore an additional aileron drag influence is introduced. Moreover lift and drag coefficient can be transformed from the aerodynamic coordinate system into the body fixed (no sideslip or side force effects) resulting in the additional X and Z force coefficients

$$\begin{aligned}\Delta C_{X\text{Ice}} = & \; \Delta C_{L\text{Ice}} \sin(\alpha) - \Delta C_{D\text{Ice}} \cos(\alpha) \\ \Delta C_{Z\text{Ice}} = & - \Delta C_{L\text{Ice}} \cos(\alpha) - \Delta C_{D\text{Ice}} \sin(\alpha).\end{aligned} \tag{31}$$

The horizontal tail is mainly influenced due to icing by changed flow due to wing icing effects and ice accretion on the surface. To consider the changed inflow, the calculation of the downwash angle ε (see Fig. 3) is extended with the additional wing lift dependent parameter

$$\frac{\partial \varepsilon_{\text{HT}}}{\partial C_{L,\text{WB}}} = d_{\frac{\partial \varepsilon_{\text{HT}}}{\partial C_{L,\text{WB}}}}. \tag{32}$$

Hence, the additional ice downwash angle is

$$\Delta \varepsilon_{\text{HTIce}} = d_{\frac{\partial \varepsilon_{\text{HT}}}{\partial C_{L,\text{WB}}}} C_{L,\text{WB}}(t - \Delta t). \tag{33}$$

It is assumed that the icing relevant horizontal tail angle of attack $\Delta\alpha_{\text{HTIce}}$ is a combination of the changed downwash and the basic model angle of attack α_{HT}:

$$\Delta \alpha_{\text{HTIce}} = \alpha_{\text{HTBase}} + \Delta \varepsilon_{\text{HTIce}}. \tag{34}$$

The icing part of the horizontal tail lift coefficient is given by

$$\begin{aligned}\Delta C_{L,\text{HTIce}} = & k_{C_{L\alpha,\text{HT}}} C_{L\alpha,\text{HTBase}} \Delta \alpha_{\text{HTIce}} \\ & + k_{C_{L\eta}} C_{L\eta\text{Base}} \eta\end{aligned} \tag{35}$$

with altered lift coefficient and elevator efficiency:

$$\begin{aligned}C_{L\eta} &= \left(1 + k_{C_{L\eta}}\right) \cdot C_{L\eta\text{Base}} \\ C_{L\alpha,\text{HT}} &= \left(1 + k_{C_{L\alpha,\text{HT}}}\right) \cdot C_{L\alpha,\text{HTBase}}.\end{aligned} \tag{36}$$

Further, $\Delta C_{L,\text{HTIce}}$ can be divided into a body fixed longitudinal and vertical force coefficient

$$\begin{aligned}\Delta C_{X\text{HTIce}} = & \; \Delta C_{L,\text{HTIce}} \sin\left(\Delta\alpha_{\text{HTIce}} - i_{\text{HT}}\right) \\ \Delta C_{Z\text{HTIce}} = & - \Delta C_{L,\text{HTIce}} \cos\left(\Delta\alpha_{\text{HTIce}} - i_{\text{HT}}\right).\end{aligned} \tag{37}$$

The pitching moment is a combination of wing, body and horizontal tail influences as given in Eq. (16). The additional icing related part results due to a changed wing/body pitch, horizontal tail force and wing separation point:

$$\begin{aligned}\Delta C_{m\text{Ice}} = \; & k_{C_{m0,\text{WB}}} C_{m0,\text{WBBase}} \\ & + \left(\frac{S_{\text{HT}}}{S_{\text{Wing}}} \frac{r^\star_{\text{HT}}}{\bar{c}} \Delta C_{Z\text{HTIce}}\right) \\ & - \left(\frac{S_{\text{HT}}}{S_{\text{Wing}}} \frac{z^\star_{\text{HT}}}{\bar{c}} \Delta C_{X\text{HTIce}}\right) \\ & + \left(k_{\frac{\partial C_m}{\partial \widehat{X}}} \left(1 - \left(\Delta \widehat{X}_{\text{Ice}} + \widehat{X}_{\text{Base}}\right)\right) \right. \\ & \qquad \left. - \Delta \widehat{X}_{\text{Ice}} \right) \left(\frac{\partial C_m}{\partial \widehat{X}}\right)_{\text{Base}}.\end{aligned} \tag{38}$$

The above derived equations of the Δ-model finally lead to a new body fixed derivative set, which must be used to calculate longitudinal and vertical aerodynamic forces as well as the pitching moment

$$\begin{aligned}C_X &= C_{X\text{Base}} + \Delta C_{X\text{Ice}} = \frac{X_{\text{A}} + \Delta X_{\text{A}}}{\bar{q} S_{\text{Wing}}} \\ C_Z &= C_{Z\text{Base}} + \Delta C_{Z\text{Ice}} = \frac{Z_{\text{A}} + \Delta Z_{\text{A}}}{\bar{q} S_{\text{Wing}}} \\ C_m &= C_{m\text{Base}} + \Delta C_{m\text{Ice}} = \frac{M_{\text{A}} + \Delta M_{\text{A}}}{\bar{q} S_{\text{Wing}} \bar{c}}.\end{aligned} \tag{39}$$

With available basic model parameter estimates held fixed, the following 18 Δ-model parameters could be estimated from flight data under icing conditions: k_{τ_2}, k_{c_1}, k_{α^*}, α_{BP}, $k_{C_{L0,\text{low}}}$, $k_{C_{L\alpha,\text{WB,low}}}$, $k_{C_{L\alpha,\text{WB,high}}}$, $k_{C_{D0}}$, d_{k_1}, d_{k_2}, k_{k_2}, d_{k_4}, $k_{\frac{\partial C_D}{\partial \widehat{X}}}$, $d_{\frac{\partial \varepsilon_{\text{HT}}}{\partial C_{L,\text{WB}}}}$, $k_{C_{L\eta}}$, $k_{C_{L\alpha,\text{HT}}}$, $k_{C_{m0,\text{WB}}}$, $k_{\frac{\partial C_m}{\partial \widehat{X}}}$.

5 FLIGHT DATA BASE

The flight data base of a light jet airplane used to identify parameters of the Δ-model is available within a joint research program between the DLR Institute of Flight Systems and EMBRAER concerning aircraft icing degradation modeling and detection. For the herein presented work different types flight data are evaluated:

1. flight data without ice accretion to identify the basic aircraft model
2. flight data with simulated ice accretion resp. two different artificial ice shape configurations

All data is collected from flights in clean configuration as well as similar altitude and speed ranges. Positions on wing and horizontal tail as well as general shape of the artificial ice accretions used to degrade the aircraft aerodynamics during flight test are given in Figs. 5 and 6. Resulting from numerical calculations of the 2D airfoil ice accretion, the 3D ice geometries for both cases had been designed. The artificial ice shapes for the flight test were mechanically produced afterwards and glued to the wing surface prior to the flights. The essential difference between both cases is that for case 1 the ice accretion is far beyond the leading edge, and for case 2 the leading edge is covered.

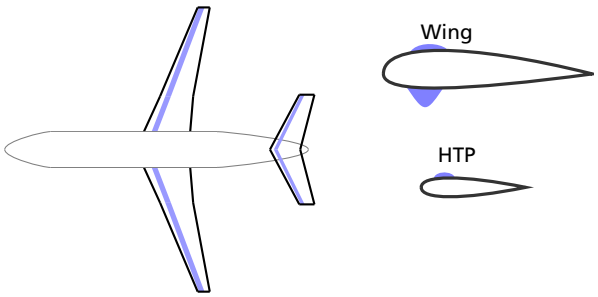

Figure 5: Illustration of artificial ice shape configuration (run-back ice, case 1)

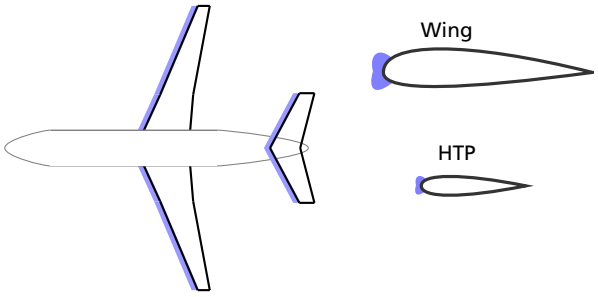

Figure 6: Illustration of artificial ice shape configuration (in-flight ice, case 2)

For the herein presented parameter estimation 29 data sets (about 2400 s recording time) containing maneuvers from flights with case 1 ice shapes are used. These include maneuvers with approaches to the stall point without a complete separation and reattachment. Due to flight safety reasons the higher angle of attack region, where a complete flow separation was anticipated, was not entered, because it could not be determined if the aircraft could be safely recovered with the ice shapes attached. After only a slight visible flow separation resp. lift loss and drag increase, the aircraft was brought back into a safe flight condition. Further 3 data sets of maneuvers from the case 2 icing flight test with length of 300 s are available mainly containing push over maneuvers, with no direct intention to approach stall.

As mentioned above, icing aerodynamic performance degradation mainly influences the aircraft drag. The complete aircraft lift and drag coefficients are calculated from the acceleration measurements by rearranging Eqs. (5) - (7)[17]. The resulting drag polars are given in Fig. 7.

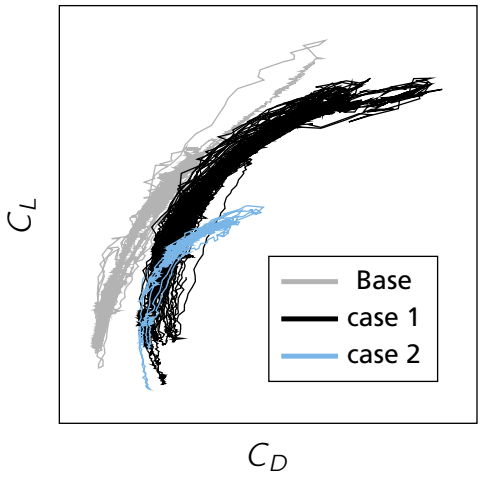

Figure 7: Measured drag polar (clean, case 1&2)

Especially for case 2, the drag coefficient behavior is far different from the basic aircraft with a significant drag increase at even lower lift coefficient values resp. angles of attack as seen from the curvature of the drag polar curves in Fig. 7. Another point is the zero drag increase which is similar for both cases and strongly influences the aircraft's dynamic behavior. These effects must be covered in the Δ-model in order to reproduce the measured aircraft motion.

All flight data records include measurements of

- translational accelerations (a_x, a_y, a_z)
- rotational rates (p, q, r)
- aircraft attitude (Φ, Θ, Ψ)
- true airspeed V_{TAS}, angle of attack α and angle of sideslip β
- geographic position (ϕ_{lat}, λ_{lon}) and altitude H
- elevator η, horizontal stabilizer i_{HT}, aileron ξ and rudder ζ deflection.

Further, post-flight calculations of

- center of gravity (x_{CG}, y_{CG}, z_{CG}), moments of inertia (I_{xx}, I_{yy}, I_{zz}, I_{xz}) and aircraft mass m
- engine thrust ($F_{E,LH}$, $F_{E,RH}$)

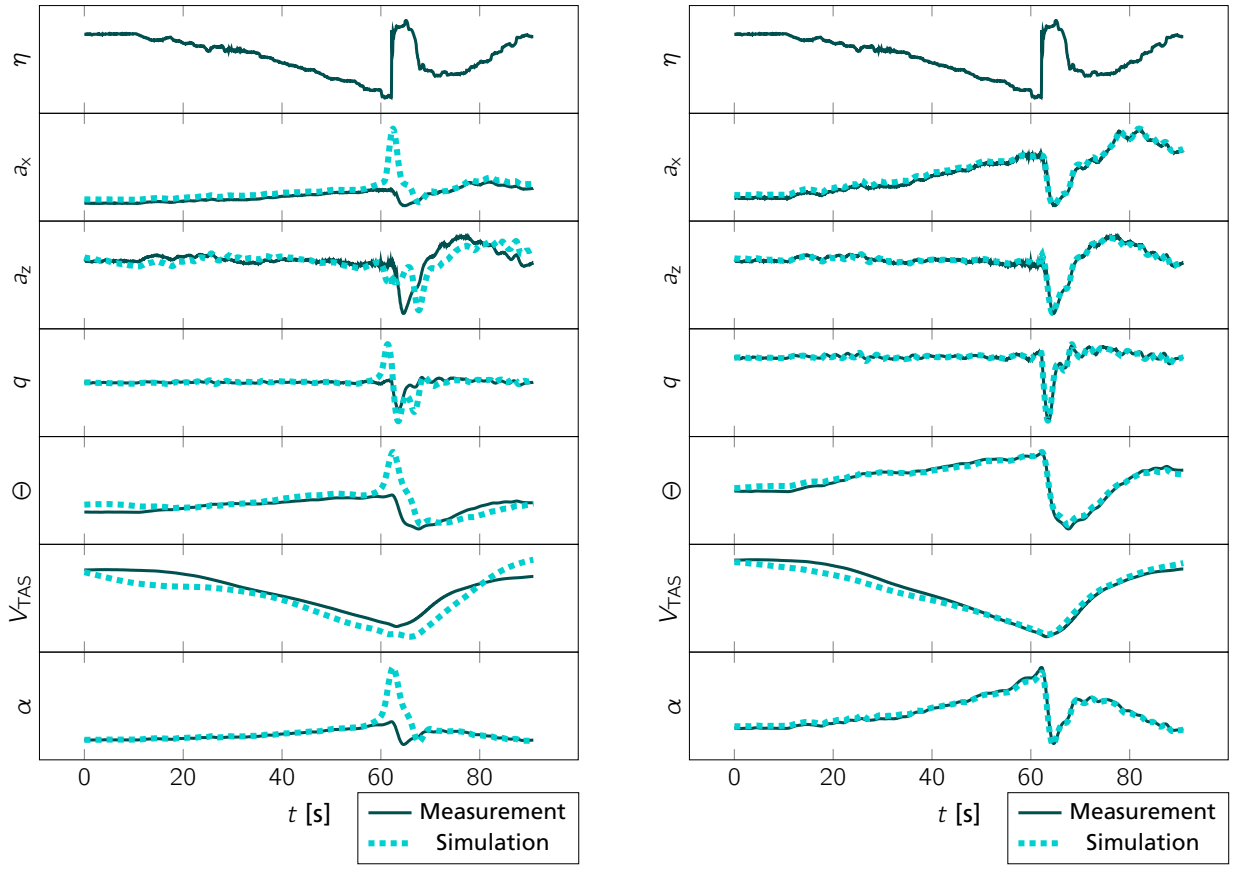

(a) without Δ-model

(b) with Δ-model

Figure 8: Time history of aircraft reaction (case 1, stall approach maneuver) – measurement and simulation of several example outputs

are available. Rotational accelerations $\dot{p}$, $\dot{q}$, $\dot{r}$ are calculated by numerical differentiation. With these channels all the information about the dynamic behavior of the aircraft is available for the parameter estimation applying the output error method in time domain.

To further guarantee the data compatibility[17], a flight path reconstruction and sensor model identification was performed. This work resulted in reliable calculation of the inflow angles (α, β) and true airspeed (V_{TAS}) at the center of gravity.

6 PARAMETER ESTIMATION RESULTS

The above derived Δ-model equations were included as a special model part in the overall aircraft simulation used for the previously conducted basic model identification. Note that this is the same model which can be used for desktop analyses and simulator trials. The model is coded in C/C++ and connected to the Fitlab estimation software environment.

The Δ-model equations only affect the longitudinal aerodynamics at this first stage. Using only longitudinal maneuvers for the parameter estimation a reduction to a longitudinal 3-DOF aircraft simulation model is reasonable. Therefore the state equations of $\dot{v}$, $\dot{p}$ and $\dot{r}$ in Eq. (5) and Eq. (7) are not evaluated and the corresponding states v, p and r are replaced by measurements. This reduction allows to still use the existing basic aerodynamic model but prevents the need for an additional Δ-model formulation of lateral motion related coefficients. The weighted model outputs for parameter estimation are a_x, a_z, Θ, q, $\dot{q}$, H, V_{TAS}, Ma and α, which contain all necessary information for the identification of the longitudinal aerodynamics.

Data of each icing case is used to separately estimate Δ-model parameters leading to two individual icing parameter sets. The estimations were successful for both icing cases and the Δ-model is able to represent the measurements quite well during the simulation. Figure 8a shows a time history plot for one example case 1 stall approach maneuver without the Δ-model extension, Fig. 8b with the

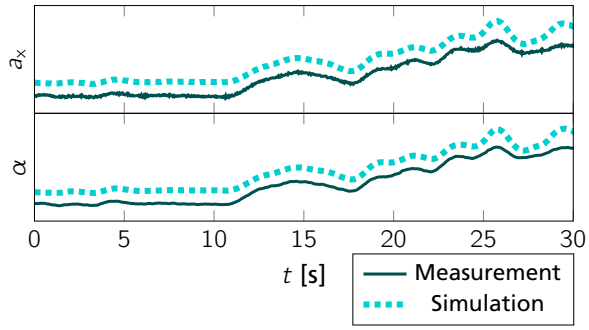

Figure 9: Time history of aircraft reaction (case 1, first 30 s of stall approach maneuver) – measurement and simulation (without Δ-model)

Δ-model. With choice of suitable initial conditions in the simulations, the basic model could only approximately match the steady flight in the beginning. The first 30 s of Fig. 8a are given in Fig. 9 for the angle of attack α and longitudinal acceleration a_x signals. The visible difference between measurement and basic model output mainly results from additional drag caused by case 1 icing.

The basic model simulation in Fig. 8a further results in a wrong dynamic behavior for higher angles of attack. With measured model control inputs similar to Fig. 4b, but icing dependent different horizontal tail trim angle, the basic model encounters an excessive pitch up at high angles of attack. The different lift, drag and pitching moment behavior of the measured degraded aircraft aerodynamics cannot be covered by the basic aerodynamic model.

Adding the herein developed Δ-model allows to suitable match the measurements during the whole maneuver (see Fig. 8b). The simulation results show that not only flight performance changes are covered (see match of longitudinal acceleration a_x and angle of attack α) but also altered dynamic pitching behavior after the push down.

Similar results are shown by the time history plot (Fig. 10) of a case 2 push over maneuver. The basic model is not able to match the measurements, especially the acceleration a_x indicating a significant drag increase cause by the ice shapes. Look-

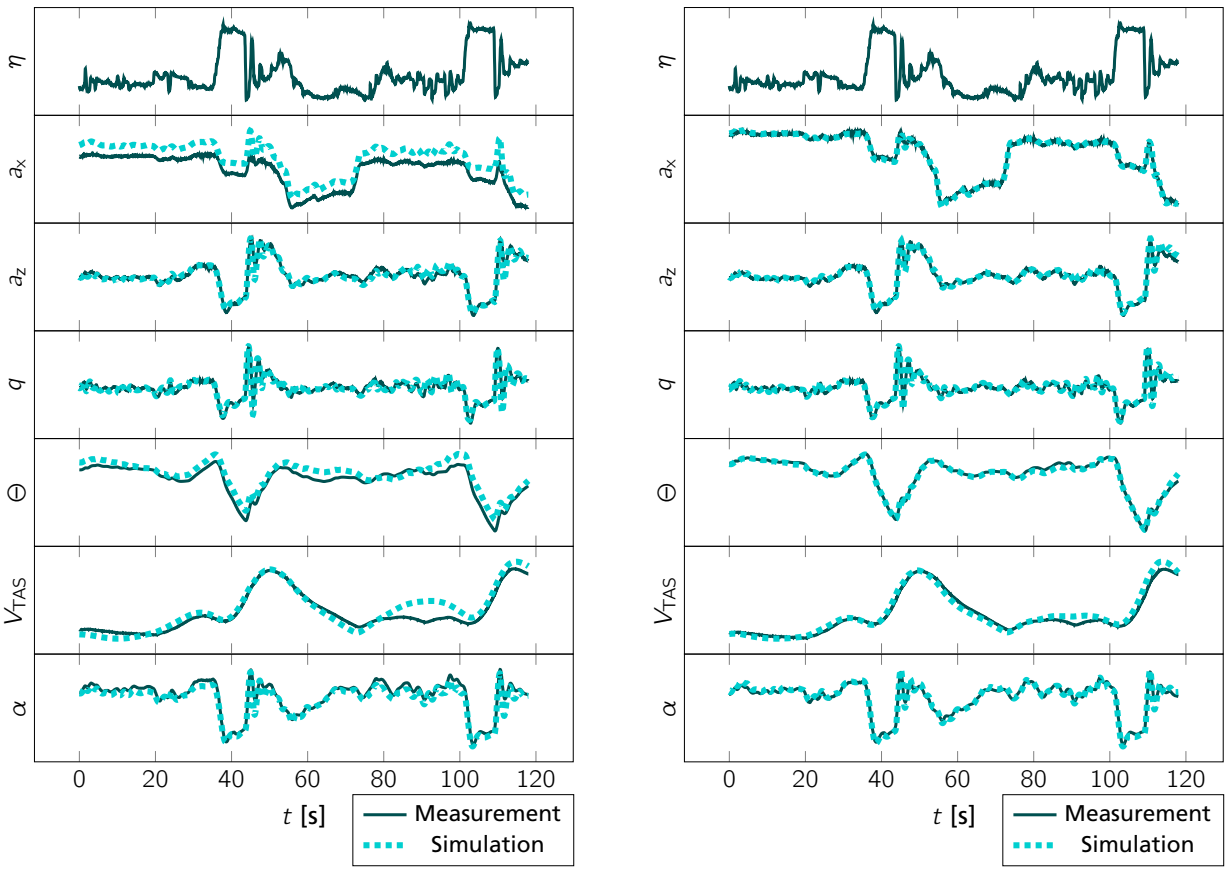

(a) without Δ-model

(b) with Δ-model

Figure 10: Time history of aircraft reaction (case 2, push over maneuver) – measurement and simulation of several example outputs

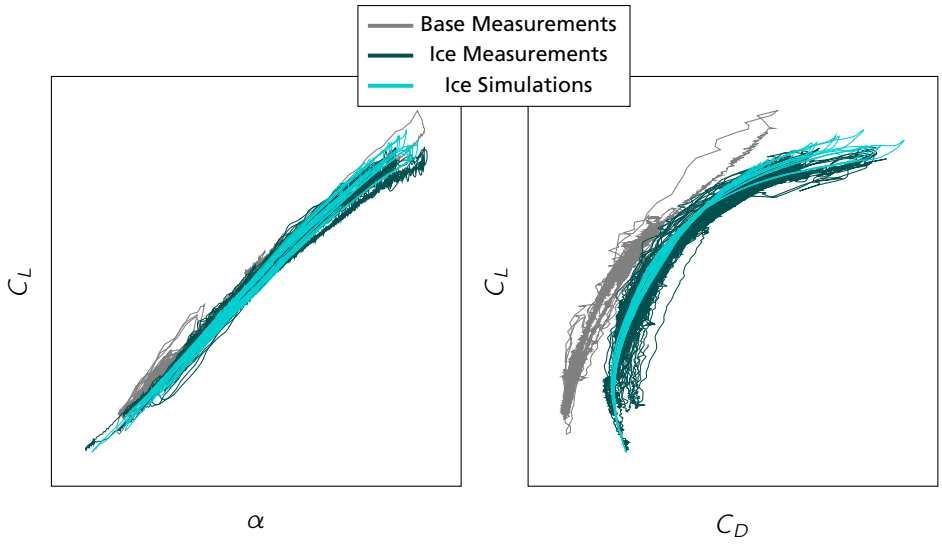

Figure 11: Lift curve and drag polar for measured and simulated data (case 1)

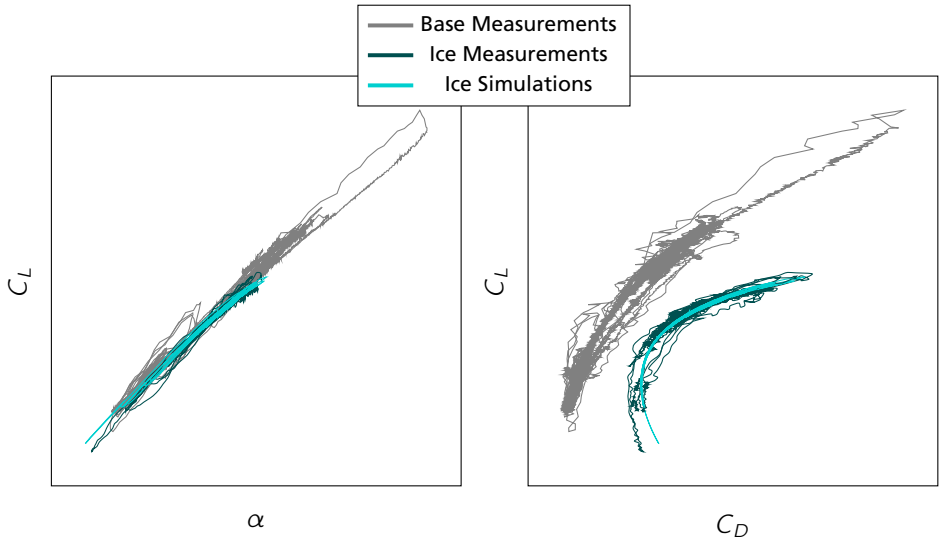

Figure 12: Lift curve and drag polar for measured and simulated data (case 2)

ing at the pitch rate q and vertical acceleration a_z indicates altered aircraft dynamics. Shortcomings of the basic model aerodynamics to cope with icing effects manifest in a poor measurements match during the elevator inputs. When adding the Δ-model, the altered aircraft's performance and dynamic motion including the ice related changes are fully covered. These example results of both cases indicate that the Δ-model approach to cover icing related aerodynamic degradation is reliable.

An additional information about the quality of the Δ-model concerning icing degradations is shown by the comparison of measured and simulated lift curve and drag polar. In Fig. 11 both are given for measured basic data, measured case 1 data and corresponding simulation results. Measured icing lift and drag coefficients are well matched by the basic model simulation with the Δ-model extension. Applying the output error method allows to not only fully cover the measured aircraft outputs, but also match the calculated aerodynamic aircraft coefficients (without channel weighting during the estimation process) allowing to physically interpret the parameter estimates by investigation the lift/drag curve changes. This combination of output and coefficient match gives an advantage over the equation error method formerly used to develop icing models [13], where aerodynamic coefficients are altered resulting in new lift and drag curves without considering the aircraft motion.

For the second icing case, a similar plot is given in Fig. 12. The match of measured and simulated complete aircraft coefficients is as good as for

case 1			case 2		
parameter	value	σ [%]	parameter	value	σ [%]
k_{τ_2}	–	–	k_{τ_2}	–	–
k_{c_1}	0.200000 *	–	k_{c_1}	0.257501	2.52
k_{α^*}	−0.010000 *	–	k_{α^*}	−0.558154	0.19
α_{BP}	0.174500 *	–	α_{BP}	–	–
$k_{C_{L0},\mathrm{low}}$	−0.232120	0.42	$k_{C_{L0},\mathrm{low}}$	–	–
$k_{C_{L\alpha,\mathrm{WB}},\mathrm{low}}$	–	–	$k_{C_{L\alpha,\mathrm{WB}},\mathrm{low}}$	–	–
$k_{C_{L\alpha,\mathrm{WB}},\mathrm{high}}$	−0.140729	0.75	$k_{C_{L\alpha,\mathrm{WB}},\mathrm{high}}$	–	–
$k_{C_{D0}}$	2.350156	0.27	$k_{C_{D0}}$	2.217056	0.56
d_{k_1}	−0.064813	0.98	d_{k_1}	−0.064807	1.30
d_{k_2}	0.870595	1.40	d_{k_2}	–	–
k_{k_2}	–	–	k_{k_2}	–	–
d_{k_4}	−0.021925	1.36	d_{k_4}	–	–
$k_{\frac{\partial C_D}{\partial \hat{X}}}$	2.120364	0.85	$k_{\frac{\partial C_D}{\partial \hat{X}}}$	−0.534473	1.10
$d_{\frac{\partial \epsilon_{\mathrm{HT}}}{\partial C_{L,\mathrm{WB}}}}$	−0.066634	0.23	$d_{\frac{\partial \epsilon_{\mathrm{HT}}}{\partial C_{L,\mathrm{WB}}}}$	–	–
$k_{C_{L\eta}}$	−0.172974	0.23	$k_{C_{L\eta}}$	−0.081780	0.68
$k_{C_{L\alpha,\mathrm{HT}}}$	−0.185360	0.13	$k_{C_{L\alpha,\mathrm{HT}}}$	–	–
$k_{C_{m0,\mathrm{WB}}}$	−3.037087	0.17	$k_{C_{m0,\mathrm{WB}}}$	–	–
$k_{\frac{\partial C_m}{\partial \hat{X}}}$	−0.099850	2.71	$k_{\frac{\partial C_m}{\partial \hat{X}}}$	−0.614451	0.23

Table 1: Δ-model parameters of both investigated icing cases – fixed values, resulting estimates and corresponding standard deviation (* fixed)

case 1. The large deviation of the case 2 drag polar from the clean measurements shows the need for additional model parts.

The corresponding Δ-model parameters are listed in Table 1 for both icing cases. The first block of parameters (k_{τ_2}, k_{c_1}, k_{α^*}) is corresponding to the flow separation model formulation. For both cases the beginning flow separation is reduced to lower angles of attack due to a negative k_{α^*} (e.g. 55 % reduction in case 2), which is consistent to the general degradation (see Fig. 1). For case 1 icing, the parameters had been fixed at particular values during the identification process to cope with the nonlinear lift slope at higher angles of attack. The slight change in α^* guarantees an earlier beginning flow separation and a good match of the lift coefficient calculated from the measurements.

Note that the flow separation model as formulated in Eqs. (8) - (16) and described in Refs. [17, 20, 21, 22] is mainly derived to cope with effects of a trailing edge flow separation moving to the leading edge with increasing angle of attack. For the available icing flight test data it cannot be determined whether the flow separation occurs in such a manner or other types of flow separation develop. For example, a separation bubble or a leading edge stall could be caused by the presence of the attached ice shapes on the wing. The model formulation in Eqs. (18) - (21) is inspired by usual flow separation behavior which can be observed on most aircraft without icing. In this preliminary analysis, the same model is applied to investigate its usability without in-depth analysis of actual aerodynamic phenomena. Using this formulation, a very good match with the flight test data was obtained during the identification process. However, there is no guarantee that the physical interpretation in terms of flow separation behavior remains valid. Similarly, the validity domain of the model is restricted to the domain covered by the flight test data.

For case 2 icing a slight nonlinearity in the (measured) lift curve is visible, which is assumed to result from beginning flow separation on the wing airfoil, indicating a strong influence on the aircraft's aerodynamics by the artificial ice shapes. Because of no complete separation could be detected in the flight data for both cases, which is consis-

tent to the flight test attempt to not fly into danger flight conditions with attached ice shapes, no hysteresis parameter could be estimated.

The second block in Table 1 contains parameters for altering the wing lift coefficient (α_{BP}, $k_{C_{L0},low}$, $k_{C_{L0},high}$, $k_{C_{L\alpha,WB},low}$, $k_{C_{L\alpha,WB},high}$). For case 1 icing a breakpoint formulation is needed to alter the lift curve according to the measurements. In this case, the breakpoint α_{BP} was previously fixed and not estimated. The gathered case 2 data contains only maneuver in the lower angle of attack region (see Fig. 12), so that the additional lift curve breakpoint formulation seemed not necessary.

For case 1, the estimated general wing lift slope decrease for higher angles of attack ($k_{C_{L\alpha,WB},high}$ behind the breakpoint) is about $14\,\%$. No lift curve change was detected in the low angle of attack region for this case, so $k_{C_{L\alpha,WB},low}$ is fixed to zero. The zero lift coefficient ($k_{C_{L\alpha,WB},low}$) is reduced about $23\,\%$, which probably results from significant icing induced wing flow changes (see ice shape configuration in Fig. 5). During the estimation process, no significant alteration parameters could be estimated for case 2. Hence, the corresponding lift derivative parameters were not estimated at all, resulting in the basic aircraft's lift curve (see Fig. 12). As stated above, the slight non-linear lift curve change at the highest measured angles of attack for this case presumably result from beginning wing flow separation.

The drag related Δ-model parameters (third block in Table 1) describe the main influence of icing on the aircraft's aerodynamics (see. Fig. 1). A zero drag increase $k_{C_{D0}}$ of more than $200\,\%$ for both cases shows the significance of the aircraft performance degradation due to icing. Due to the significant difference in the drag polar curvature from the base model quadratic polar formulation further drag related parameters (d_{k_1}, d_{k_2}, k_{k_2}, d_{k_4} and $k_{\frac{\partial C_D}{\partial \widehat{X}}}$) had to be introduced to match the altered drag curves in presence of icing (see. Figs. 11 and 12).

As usual in system identification, the choice of a model structure and a parameter set is empirical driven by the effects visible in the gathered data. Engineer's knowledge and understanding of the physics can be introduced in the model structure by defining parameters to which simple physical interpretations can be linked. Physics-based parameter often admit simple relationships and strengthen the understanding of the engineer: For instance the quadratic relationship between lift and induced drag can usually be observed on clean aircraft. For similar lift coefficients in the clean and icing case, the induced drag due to this effect should not significantly differ in both cases. The presence of protuberances (ice accretions) on the wing, as for case 1 (see Fig. 5), causes a significant increase of the zero lift drag C_{D0} and further drag increases with the angle of attack can also be expected. To describe further dependencies in the correlation of angle of attack, lift and induced drag (see Fig. 11) the additional parameters or changes d_{k_1}, d_{k_2}, d_{k_4} (k_{k_2} is not estimated) in table 1 are introduced for case 1.

Indeed, it can be observed in the data that both the zero lift drag and the drag dependency on lift are massively increased (especially in case 2), which justifies the use of additional parameters ($k_{C_{D0}}$, $k_{\frac{\partial C_D}{\partial \widehat{X}}}$) to model this effect. As already mentioned the physical interpretation in terms of flow separation point [20] that is usually associated with $\widehat{X}$ is probably not valid in case 2.

Changes of the downwash angle to account for the changed flow behind the wing because of the attached ice shapes are represented by the parameter $d_{\frac{\partial \epsilon_{HT}}{\partial C_{L,WB}}}$ in the fourth block of Table 1. A separation of the physical effects of downwash, horizontal tail and wing pitching moment in the estimated parameters is difficult without an additional information about the horizontal tail angle of attack. Therefor an interpretation of the resulting minor downwash decrease for case 1 is not possible with the available information. Further a degradation of the elevator efficiency by $17\,\%$ (case 1) resp. $8\,\%$ (case 2) is detectable ($k_{C_{L\eta}}$, block 5 in Table 1). This could be explained by a changed flow over the elevator caused by the attached ice shapes and the found degradation is comparable to e.g. the findings in [8]. The reduced horizontal lift tail lift slope $k_{C_{L\alpha,HT}}$ in case 1 (about $19\,\%$) may result from over the wing ice shapes (see Fig. 5), but this can not be completely determined here, because as previously stated, without measurement of the angle of attack at the horizontal tail it is not possible to reliably separate tailplane influences from other effects.

In the last block of Table 1 the pitching moment coefficient changes ($k_{C_{m0,WB}}$, $k_{\frac{\partial C_m}{\partial \widehat{X}}}$) are listed. The reduction of the zero moment coefficient relative to the base model parameters $k_{C_{m0,WB}}$ of about $300\,\%$ for case 1, corresponding to a horizontal tailplane trim angle change Δi_{HT} of $0.5°$. With ice accumulations on the wings a changed flow and therefore changed wing pitching behavior is expectable. Also some horizontal tailplane and downwash influences can be included in this parameter, as stated above, it is difficult to sepa-

rate various effects in the estimation without a tailplane angle of attack measurement. The parameter $k_{\frac{\partial C_m}{\partial \dot{X}}}$ may further mathematically compensate some effects to obtain a good match.

The relative standard deviation σ of the estimates give an impression about the parameter identifiability and estimation quality. For case 1 nearly all estimates show a small relative standard deviation. Note that k_{c_1}, k_{α^*} and α_{BP} had been set to the values given in table 1 and were fixed during the estimation. Only the estimate $k_{\frac{\partial C_m}{\partial \dot{X}}}$ seems to be questionable, but was found very helpful to fit the measurements during the estimation. Further, the relative standard deviations σ of the case 2 parameter estimates are comparable to case 1 and in general small enough to trust the parameter results. With only 3 maneuver sets available it was difficult to match the measurements of aircraft outputs (Fig. 10) and lift/drag curves (Fig. 12) with the given parameters. It is assumed that with more data available, the standard deviation could be further reduced or a different parameter set could be found describing the measurements.

Overall, the parameter estimation results of the Δ-model for different ice cases show that the additional model is needed to match the measurements of the altered aircraft steady and dynamic behavior due to icing on wing and horizontal tailplane. Moreover, several major effects of icing can be detected in the flight data and are represented by the developed Δ-model:

case 1 (run-back ice):

- significant drag increase, especially at zero lift
- non-linear lift curve with presumed maximum lift coefficient $C_{L,\max}$ at angles of attack below the clean aircraft $\alpha_{\max}$
- significant reduction of elevator control efficiency

case 2 (in-flight ice):

- significant drag increase, especially at zero lift and angles of attack far below clean aircraft's $\alpha_{\max}$
- non linear lift curve with presumed maximum lift coefficient at angles of attack below half of clean aircraft $\alpha_{\max}$

7 SUMMARY

In this paper a new approach to model aerodynamic degradation effects in an aircraft simulation and the time domain estimation of the corresponding parameters is presented . The Δ-model approach is an extension of the basic aircraft model and usable as an individual module for the simulation in e.g. a research or training simulator. It is analytically derived from a two point aerodynamic model formulation including stall. In the presented stage it reliably describes changes of the longitudinal aircraft aerodynamics.

Using flight data without and with two artificial ice shape configurations on wing and horizontal tail (available at DLR Institute of Flight Systems due to a cooperation with EMBRAER) parameters of the Δ-model were identified. Comparison of simulations with and without the Δ-model show the necessity of the additional model part to cover changes in the aircraft behavior and the capability to match the measurements. The advantage of the estimation method is visible in proof of match plots for various measured outputs of the dynamic system showing that the extended model delivers well comparable time histories.

Further, several resulting parameter values could be interpreted according to the main ice influences on the aircraft's aerodynamics allowing general conclusions of ice related degradation on the aircraft behavior. As a primary effect of icing, the significant drag increase with ice accumulation on certain aircraft surfaces is clearly visible in values of drag related delta model parameters giving a clue about the amount of drag increase and shape of the altered drag polar.

8 FUTURE WORK

In future work, the Δ-model will be extended in several ways. The alteration of the longitudinal derivative model could be augmented by a lateral aerodynamic part also changing the side force, rolling and yawing coefficient. Another possibility is to introduce a separation of the different aerodynamic surfaces in the model, e.g. dividing the wing into a left and right part and calculating additional individual forces. This will have the advantage to also simulate asymmetric ice accretions as they happened in various icing related accidents in the past, which is considered to be highly beneficial for pilot training. For lateral dynamics, estimation of reduced control surface efficiencies (ailerons, spoilers) is necessary to obtain a complete model influencing all 6 degrees of freedom.

ACKNOWLEDGEMENT

The author wants to thank the colleagues of EMBRAER for pushing forward the joint research on aircraft icing and supplying the flight test data analyzed in this paper. Further, the model development is part of the DLR@Uni project "Supercooled Large Droplet Icing", a joint research project of several DLR and university institutes in Braunschweig.

References

[1] Green, Steven D.: *A Study of U. S. Inflight Icing Accidents and Incidents, 1978 to 2002*. 44th AIAA Aerospace Sciences Meeting and Exhibit, Reno, Nevada, USA, January 9th - 12th, 2006. American Institute of Aeronautics and Astronautics, Inc. (AIAA), Paper No. AIAA 2006-82.

[2] N.N., *Final Report (BFU 5X011-0/98)*. Bundesstelle für Flugunfalluntersuchung, April, 2001, Braunschweig, DE.

[3] N.N., *Aircraft Accident Report (NTSB/AAR-96/01, DCA95MA001), Safety Board Report*. National Transportation Safety Board (NTSB), July 9th, 1996, Washington, DC, USA.

[4] Gray, Vernon H.: *Prediction of aerodynamic penalties caused by ice formations on various airfoils*. Technical Note D-2166, National Aeronautics and Space Administration (NASA), Washington, D.C., USA, Februar, 1964.

[5] N.N.: *Ice Accretion Simulation*. AGARD Advisory Report 344, Advisory Group for Aerospace Research & Development (AGARD) - Fluid Dynamics Panel Working Group 20, North Atlantic Treaty Organization (NATO), Neuilly-Sur-Seine, France, December, 1997.

[6] Broeren, Andy P.; Whalen, Edward A.; Busch, G. T. and Bragg, Michael B.: *Aerodynamic Simulation of Runback Ice Accretion*. Journal of Aircraft, Vol. 47, No. 3, pp. 924–939, May-June, 2010.

[7] Ranuado, Richard J.; Batterson, J. G.; Reehorst, A. L.; Bond, T.H. and O'Mara, T. M.: *Determination Of Longitudinal Aerodynamic Derivatives Using Flight Data From An Icing Research Aircraft*. 27th AIAA Aerospace Science Meeting, Reno, Nevada, USA, January 9th - 12th, 1989. American Institute of Aeronautics and Astronautics, Inc. (AIAA), Paper No. AIAA 89-0754.

[8] Ratvasky, Thomas P. and Ranuado, Richard J.: *Icing Effects on Aircraft Stability and Control Determined from Flight Data. Preliminary Results*. 31st AIAA Aerospace Science Meeting and Exhibit, Reno, Nevada, USA, January 11th - 14th, 1993. American Institute of Aeronautics and Astronautics, Inc. (AIAA), Paper No. AIAA 93-0398.

[9] Lee, Sam; Barnhart, Billy P. and Ratvasky, Thomas P.: *Dynamic Wind-Tunnel Testing of a Sub-Scale Iced S-3B Viking*. AIAA Atmospheric and Space Environments Conference, Toronto, Ontario Canada, August 2th - 5th, 2010. American Institute of Aeronautics and Astronautics, Inc. (AIAA), Paper No. AIAA 2010-7986.

[10] Gingras, David R.: *Requirements and Modeling of In-flight Icing Effects for Flight Training*. AIAA Modeling And Simulation Technologies (MST) Conference, Boston, Massachusetts, USA, August 19th - 22th, 2013. American Institute of Aeronautics and Astronautics, Inc. (AIAA), Paper No. AIAA 2013-5075.

[11] Bragg, Michael B.; Hutchison, Tim; Merret, Jason; Oltman, R. and Pokhariyal, Davesh: *Effect of Ice Accretion on Aircraft Flight Dynamics*. 38th AIAA Aerospace Science Meeting and Exhibit, Reno, Nevada, USA, January 10th - 13th, 2000. American Institute of Aeronautics and Astronautics, Inc. (AIAA), Paper No. AIAA 2000-0360.

[12] Brown, Anthony P.: *Negative Speed Stability, a Factor in Transport Airplane Icing Upsets*. 20th AIAA Applied Aerodynamics Conference, St. Louis, Missouri, USA, June 24th - 26th, 2002. American Institute of Aeronautics and Astronautics, Inc. (AIAA), Paper No. AIAA 2002-3051.

[13] Deters, Robert W.; Dimock, Glen A. and Selig, Michael S.: *Icing Encounter Flight Simulator*. Journal of Aircraft, Vol. 43, No. 5, pp. 1528–1537, September, 2006.

[14] Lampton, Amanda and Valasek, John: *Prediction of Icing Effects on the Dynamic Response of Light Airplanes*. Journal of Guidance, Control, and Dynamics, Vol. 30, No. 3, pp. 722–732, May-June, 2007.

[15] Ratvasky, Thomas P.; Barnhart, Billy P.; Lee, Sam and Cooper, Jon: *Flight Testing an Iced Business Jet for Flight Simulation Model Validation*. 45st AIAA Aerospace Science Meeting and Exhibit, Reno, Nevada, USA, January 8th - 11th,

2007. American Institute of Aeronautics and Astronautics, Inc. (AIAA), Paper No. AIAA-2007-0089.

[16] Whalen, Edward A.; Lee, Sam; Bragg, Michael B. and Ratvasky, Thomas P.: *Characterizing the Effect of Ice on Aircraft Performance and Control from Flight Data*. 40th AIAA Aerospace Sciences Meetings and Exhibit, Reno, Nevada, USA, January 14th - 17th, 2002. American Institute of Aeronautics and Astronautics, Inc. (AIAA), Paper No. AIAA 2002-0816.

[17] Jategaonkar, Ravindra V.: *Flight Vehicle System Identification - A Time Domain Methodology: Second Edition*, volume 245 of *Progress in Astronautics and Aeronautics*. American Institute of Aeronautics and Astronautics, Inc., 1801 Alexander Bell Drive, Reston, Virginia 20191, USA, 2015.

[18] Mönnich, Wulf: *Ein 2-Punkt-Aerodynamikmodell für die Identifizierung*. Symposium 'Systemidentifizierung in der Fahrzeugdynamik'. DFVLR Mitteilung 87-22, Paper No. 3.1, 1987, in German.

[19] Hamel, Peter G. and Jategaonkar, Ravindra V.: *Evolution of Flight Vehicle System Identification*. Journal of Aircraft, Vol. 33, No. 1, pp. 9–28, January-February, 1996.

[20] Fischenberg, Dietrich: *Identification of an unsteady aerodynamic stall model from flight test data*. AIAA Atmospheric Flight Mechanics Conference, pages 138–146, Baltimore, Maryland, USA, August 7th - 10th, 1995. American Institute of Aeronautics and Astronautics, Inc. (AIAA), Paper No. AIAA 95-3438-CP.

[21] Fischenberg, Dietrich and Jategaonkar, Ravindra V.: *Identification of Aircraft Stall Behavior from Flight Test Data*. RTO - MP - 11. Paper No. 17, March, 1999.

[22] Jategaonkar, Ravindra; Fischenberg, Dietrich and Gruenhagen, Wolfgang von: *Aerodynamic Modeling and System Identification from Flight Data-Recent Applications at DLR*. Journal of Aircraft, Vol. 41, No. 4, pp. 681–691, July-August, 2004.

[23] Bragg, Michael B.: *Aircraft Aerodynamic Effects Due To Large Droplet Ice Accretions*. 34th AIAA Aerospace Sciences Meeting and Exhibit, Reno, Nevada, USA, Januar 15th - 18th, 1996. American Institute of Aeronautics and Astronautics, Inc. (AIAA), Paper No. AIAA 96-0932.